Acta Pharmaceutica Sinica B 2021;11(11):3655−3664

Chinese Pharmaceutical Association
Institute of Materia Medica, Chinese Academy of Medical Sciences

Acta Pharmaceutica Sinica B

www.elsevier.com/locate/apsb
www.sciencedirect.com

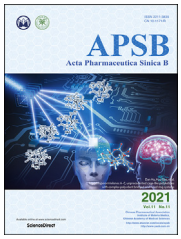

ORIGINAL ARTICLE

Tricarbocyclic core formation of tyrosine-decahydrofluorenes implies a three-enzyme cascade with XenF-mediated sigmatropic rearrangement as a prerequisite

Zhiguo Liu[a,†], Wei Li[b,c,†], Peng Zhang[b], Jie Fan[b], Fangbo Zhang[a], Caixia Wang[a], Shuming Li[d], Yi Sun[a,*], Shilin Chen[a,*], Wenbing Yin[b,c,*]

[a]*Institute of Chinese Materia Medica, China Academy of Chinese Medical Sciences, Beijing 100700, China*
[b]*State Key Laboratory of Mycology, CAS Key Laboratory of Microbial Physiological and Metabolic Engineering, Institute of Microbiology, Chinese Academy of Sciences, Beijing 100101, China*
[c]*Savaid Medical School, University of Chinese Academy of Sciences, Beijing 100049, China*
[d]*Institut für Pharmazeutische Biologie und Biotechnologie, Fachbereich Pharmazie, Philipps-Universität Marburg, Marburg 35037, Germany*

Received 19 January 2021; received in revised form 5 March 2021; accepted 16 March 2021

KEY WORDS

Tyrosine-decahydrofluorene;
Biosynthesis;
PKS−NRPS;
Xenoacremone;
Heterologous expression

Abstract Tyrosine-decahydrofluorene derivatives feature a fused [6.5.6] tricarbocyclic core and a 13-membered *para*-cyclophane ether. Herein, we identified new xenoacremones A, B, and C (**1**−**3**) from the fungal strain *Xenoacremonium sinensis* ML-31 and elucidated their biosynthetic pathway using gene deletion in the native strain and heterologous expression in *Aspergillus nidulans*. The hybrid polyketide synthase−nonribosomal peptide synthetase (PKS−NRPS) XenE together with enoyl reductase XenG were confirmed to be responsible for the formation of the tyrosine-nonaketide skeleton. This skeleton was subsequently dehydrated by XenA to afford a pyrrolidinone moiety. XenF catalyzed a novel sigmatropic rearrangement to yield a key cyclohexane intermediate as a prerequisite for the formation of the multi-ring system. Subsequent oxidation catalyzed by XenD supplied the substrate for XenC to link the *para*-cyclophane ether, which underwent subsequent spontaneous Diels−Alder reaction to give the end products. Thus, the results indicated that three novel enzymes XenF, XenD, and XenC coordinate

*Corresponding author. Tel./fax: +86 10 64013996.
E-mail addresses: ysun@icmm.ac.cn (Yi Sun), slchen@icmm.ac.cn (Shilin Chen), yinwb@im.ac.cn (Wenbing Yin).
†These authors made equal contributions to this work.
Peer review under responsibility of Chinese Pharmaceutical Association and Institute of Materia Medica, Chinese Academy of Medical Sciences.

https://doi.org/10.1016/j.apsb.2021.03.034

to assemble the [6.5.6] tricarbocyclic ring and *para*-cyclophane ether during biosynthesis of complex tyrosine-decahydrofluorene derivatives.

1. Introduction

Filamentous fungi are known to produce a variety of polyketide−nonribosomal peptide (PK−NRP) hybrids with diverse structures and extensive biological activities[1]. The subfamily of tyrosine-decahydrofluorene derivatives includes GKK1032A_2[2], hirsutellone B[3], and pyrrocidine B[4,5] that are relatively rare and specific structures (Fig. 1A). These compounds share a 13-membered *para*-cyclophane ether generated from L-tyrosine crosslinked to a fused [6.5.6] tricarbocyclic core and a hydroxypyrrolidinone moiety and are detected in various fungal species, such as *Neonectria ramulariae*[6,7], *Acremonium zeae*[8], *Hirsutella* spp[3,9], *Cordyceps sinensis*[10], and *Penicillium* spp[11,12]. These derivatives have potential antitumor, antifungal, antibacterial, antituberculosis, and enzyme-inhibiting activities[3,5,13].

Biosynthetic mechanisms of these unique multi-cyclic PKS−NRPS metabolites have attracted considerable attention. Interesting hirsutellone structures have been successively synthesized by chemists *via* various strategies[14−19]. The tricarbocyclic core was proposed to be synthesized by assembling fungal biosynthetic gene clusters[20]. Early isotope labeling studies demonstrated that L-tyrosine and an extended polyketide chain are the precursors of biosynthesis, suggesting that a hybrid polyketide synthase−nonribosomal peptide synthetase (PKS−NRPS) is responsible for the formation of the skeleton[20]. The phenolic hydroxyl group of L-tyrosine supplies the oxygen to form *para*-cyclophane according to the results of the double labeling experiments using ^{18}O,^{13}C-L-tyrosine[21]. Biosynthesis by PKS−NRPS includes elongation of the acetyl-CoA starter units by the ketosynthase domain (KS) and subsequent binding to the acyl transferase domain (AT) of acyl carrier protein (ACP). Ketoreductase (KR), dehydratase (DH), and enoyl reductase (ER) domains mediate β-keto processing steps after elongation. Ethyl groups are installed by the *C*-methyltransferase domain of PKS. The amino-acid unit is selected by the NRPS adenylation (A) domain and activated by the thiolation (T) domain. *N*-Acylation is catalyzed by the condensation (C) domain. The reductase domain (R) or Dieckmann cyclization domain (DKC) catalyzes the release of the acyl-tetramic acid derivatives. Hybrid PKS−NRPS usually do not have an ER domain; however, an individual ER domain as an independent gene is responsible for the catalytic release function in the cluster[22,23]. The PKS−NRPS assembly line and associated tailoring enzymes produce diverse structures in fungi[22]. A similar tricyclic system is present in ikarugamycin; in this case, the formation of the cyclohexene moiety was proposed to involve Diels−Alder reaction; however, enzymes catalyzing the cyclization reaction have not been reported[20].

The formation of all ring systems during biosynthesis of tyrosine-decahydrofluorene derivatives was hypothesized to include a reduction of the [6.5.6] tricarbocyclic system *via* an electrophilic cyclization and complex intramolecular Diels−Alder cyclization. A P450-catalyzed cyclization mechanism was proposed for the formation of the *para*-cyclophane moiety from the acyclic PK−NRP intermediate product. Three main cyclization mechanisms have been proposed based on the characteristics of the multiring systems[20,21,24] (Fig. 1B). In routes i and ii, electrophilic cyclization of the A-ring and the formation of *para*-cyclophane ether occur either stepwise or simultaneously to afford the Diels−Alder substrate[24,25]. Route iii suggests concomitant cyclization toward the three-ring system[20]. Detection of the corresponding intermediates is required to confirm these cyclization mechanisms. However, these intermediates are structurally complex. Moreover, detailed genetic or enzymatic investigations to support these hypotheses have not been performed in a matching fungus.

In this study, we identified three novel tyrosine-decahydr ofluorene derivatives, xenoacremones A−C (**1**−**3**) from a plant entophytic fungus *Xenoacremonium sinensis* ML-31. The fungal genetic transformation system in *X. sinensis* was established to confirm the involvement of a PKS−NRPS gene cluster (*xen*) in the biosynthesis of xenoacremones. Heterologous expression (HEx) in *Aspergillus nidulans* transformants was used to identify the key intermediates **5**, **6**, and **7**, demonstrating the roles of the cyclohexane intermediates in the formation of the multi-ring systems of xenoacremones. Finally, we demonstrated that three new enzymes, XenC, XenD and XenF, cooperate to catalyze the formation of macrocyclic ether and [6.5.6] tricarbocyclic ring of **1**. These results expand the understanding of the biosynthesis of complex tyrosine-decahydrofluorenes in fungi.

2. Materials and methods

2.1. Strains and culture conditions

All fungal strains used in the present study are listed in Supporting Information Table S1. *X. sinensis* ML-31 was used as the parental strain for gene cloning and gene deletion experiments. This strain was cultivated to determine the production of secondary metabolites in rice medium for 7 days at 25 °C. *A. nidulans* LO8030, a heterologous expression host strain, was grown at 37 or 25 °C for 3−7 days on glucose minimal medium (GMM) containing glucose (10 g/L), salt solution (50 mL/L), trace elements solution (1 mL/L), and agar (10 g/L) to collect the spores; the transformants were grown in the presence of appropriate supplements (0.5 g/L uridine, 0.5 g/L uracil, 0.65 μmol/L riboflavin, and/or 0.5 μmol/L pyridoxine HCl)[26]. *Saccharomyces cerevisiae* BJ5464-NpgA (*MATα ura3-52 his3-Δ200 leu2-Δ1 trp1 pep4::HIS3 prb1 Δ1.6R can1 GAL*) was used as the yeast assembly host to construct the expression vectors. This strain was cultured on yeast extract peptone dextrose (YPD) medium at 30 °C. *S. cerevisiae* mutants were screened on synthetic dextrose complete (SDCt) medium at 30 °C with appropriate supplements according to the auxotrophic markers introduced by transformation[27]. *Escherichia coli* DH5α were grown in Luria-

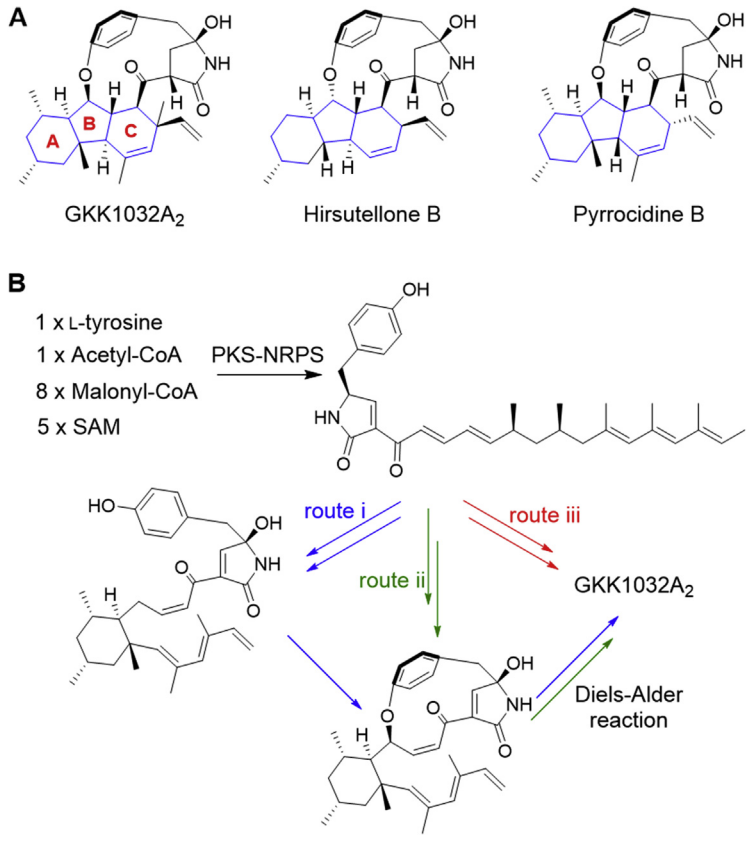

Figure 1 Representative tyrosine-decahydrofluorene structures and proposed routes of their formation. (A) Representative tyrosine-decahydrofluorene derivatives in fungi. (B) The formation routes of the derivatives proposed in previous studies.

Bertani (LB) medium (10 g/L NaCl, 10 g/L tryptone, and 5 g/L yeast extract) at 37 °C according to the DNA manipulation protocol. Ampicillin (50 μg/mL) was added for cultivation of recombinant strains of *E. coli*.

2.2. *Genome sequencing and xen gene cluster analysis*

Genome sequencing of *X. sinensis* ML-31 was performed using an Illumina HiSeq2500 by PE125 strategy at the Beijing Novogene Bioinformatics Technology Co., Ltd., and the filtered reads were assembled by SOAPdenovo to generate the scaffolds. AntiSMASH was used for initial prediction and analysis of the gene clusters for biosynthesis of secondary metabolites (http://antismash.secondarymetabolites.org/)[28]. On-line BLAST was used for functional prediction of open reading frames (ORFs) encoding proteins of the *xen* cluster (http://blast.ncbi.nlm.nih.gov). The genes of the *xen* cluster were named *xenA-G* (Supporting Information Fig. 3A). The accession number for *xen* cluster in the GeneBank database at NCBI is MT876600.

2.3. *Isolation of genomic DNA*

The hyphae of all strains of *X. sinensis* and *A. nidulans* were harvested by centrifugation at 12,000 rpm for 5 min in 2 mL Eppendorf tubes. Three steel beads (2 mm in diameter) and 700 μL of LETS buffer containing Tris-HCl (10 mmol/L), pH 8.0, EDTA (20 mmol/L), 0.5% SDS, and LiCl (0.1 mol/L) were added to the Eppendorf tubes. Phenol/chloroform/isoamyl alcohol (25:24:1) mixture (700 μL) was added to remove the protein. The mixture was sufficiently mixed and centrifuged at 12,000 rpm and 4 °C for 10 min. The supernatant containing genomic DNA was precipitated by 700 μL of 95% ethanol, and the samples were centrifuged at 13,000 rpm for 10 min. gDNA was dissolved in 50 μL of TE buffer and washed with 70% ethanol by centrifugation at 12,000 rpm and 4 °C for 3 min[26].

2.4. *PCR amplification*

PCR amplifications was performed using a T100TM Thermal cycler (Bio-Rad). High-fidelity DNA polymerases, including TransStart® FastPfu DNA polymerase (Transgene Biotech) and Phusion® high-fidelity DNA polymerase (New England Biolabs), were used to clone the genes or gene fragments. PCR reaction mixtures and thermal profiles were selected according to the manufacturer's instructions. PCR screening of the transformants was performed by using a 2X Taq Mix kit (TIANGEN BIOTECH). All primers are listed in Supporting Information Table S3. The restriction enzymes used in the study were obtained from New England Biolabs.

2.5. *Construction of deletion cassettes*

Deletion cassettes of the *xen* biosynthetic cluster genes were constructed to knock out the target genes and identify the genes and their functions by the double-joint method as described previously[32]. Gene deletion cassettes contained the upstream and downstream sequences (approximately 1.4 kb) of the target genes were linked as homologous arms to hygromycin B resistance gene

of the pUCH2-8 plasmid (approximately 2440 bp). The upstream and downstream homologous arms fragments of the genes of the *xen* cluster were amplified by PCR using a high-fidelity DNA polymerase, and the designed primers are listed in Supporting Information Fig. S2A and Table S3.

2.6. Construction of the plasmids for heterologous expression

All plasmids are listed in Supporting Information Table S2. The primers designed for heterologous expression of the genes in *A. nidulans* are listed in Table S3. Plasmid preparation, digestion with restriction enzymes, and gel electrophoresis were performed by standard methods. The coexpression strategy of the *xen* genes involved the construction of the plasmids for heterologous expression in *A. nidulans* is shown in Supporting Information Fig. S3A. Yeast assembly approach was used as described previously[29]. The pWY25.16, pYWL27 and pYWB2 plasmids were used to construct the expression vectors, as shown in Table S2. The gDNA fragments containing the *xenA-xenG* genes were amplified from gDNA of *X. sinensis* ML-31 using Phusion® high-fidelity DNA polymerase and the corresponding primers, as shown in Table S3. The transformation of *S. cerevisiae* BJ5464-NpgA was carried out according to the manufacturer's protocol for an S.c.EasyComp transformation kit (Invitrogen). Yeast colonies were screened by PCR, and the plasmids were isolated using a Zymoprep kit (D2001, Zymo Research). The yeast plasmids were transformed into *E. coli* DH5α to obtain the plasmids used for verification and subsequent transformation into *A. nidulans*.

2.7. Transformation and gene deletion in X. sinensis ML-31

A homologous recombination strategy was used for deletion of the *xen* genes in *X. sinensis* ML-31. The method of protoplast transformation was described previously[15]. *X. sinensis* ML-31 mycelia were collected from the cultures on PDA (potato dextrose agar, BD) medium after 5 days of incubation at 28 °C, and were induced in potato dextrose broth at 150 rpm/min at 28 °C for 3−4 days. Mycelia were harvested and washed with sterilized water. Then, the mycelia were resuspended in enzyme solution containing lysing enzymes (30 mg/mL) and Yatalase (20 mg/mL) in osmotic medium containing 1.2 mol/L $MgCl_2$ and 10 mmol/L sodium phosphate (pH 5.8) at 28 °C for approximately 10 h. Protoplasts were harvested using trapping buffer (0.6 mol/L sorbitol and 0.1 mol/L Tris-HCI, pH 7.0) and subsequent treatment with STC buffer (1.2 mol/L sorbitol and 0.1 mol/L Tris-HCI, pH 7.0), successively. Protoplasts were gently mixed with DNA fragments and incubated for 50 min on ice. PEG 6000 solution (1.25 mL containing 50 mmol/L $CaCl_2$, 60% PEG 6000, and 50 mmol/L Tris-HCI, pH 7.5) was added to 100 μL of the protoplasts and incubated at 25 °C for 20 min; then, the samples were plated on regeneration medium (PDA containing 1.2 mol/L sorbitol and 30 μg/mL hygromycin B). Positive colonies were selected after culture on PDA medium containing hygromycin B at 28 °C for 5 days. The deletion transformants were inoculated on PDA medium containing 30 μg/mL hygromycin B. All mutants were verified by PCR with the corresponding primers (Fig. S2 and Table S3). The rice medium was used to culture the gene deletion mutants at 25 °C for 7 days, and the production of the secondary metabolites was analyzed by LC−MS.

2.8. Transformation and heterologous expression in A. nidulans

A. nidulans LO8030 was used as the heterologous expression host strain[30]. Protoplast preparation and transformation protocols for this strain were described previously[4]. Plasmids containing the *xen* cluster genes were transformed into *A. nidulans* to generate various mutant strains (Supporting Information Table S1). Potential positive mutants were verified by PCR using the corresponding primers (Table S3). Rice medium was used to culture the verified mutants at 25 °C for 7 days for LC−MS analysis of the secondary metabolites.

2.9. General procedures for chemical analyses

LC−MS and HR ESIMS analyses were determined using a Waters-Vion-IMS-QTof system with an Electrospray ionization (ESI) source and a Waters ACQUITY UPLC® BEH column (1.7 μm, C18, 2.1 mm × 100 mm ID). The solvent gradient of 20%−95% MeCN/H_2O (both components contained 0.1% formic acid, *v/v*) was run for 23 min at a flow rate of 0.4 mL/min and was followed by elution with 95% MeCN/H_2O for 5 min. NMR spectra were determined on a Bruker AV-600 NMR spectrometer. ODS packs were obtained from YMC Co., Ltd. (Kyoto, Japan). Sephadex LH-20 was purchased from GE. Reverse phase HPLC isolation was performed using a Shimadzu LC-20AT liquid chromatograph equipped with a YMC C18 column (250 mm × 10 mm, 5 μm). Ethyl acetate (EtOAc) used for extraction was of analytical grade. HPLC grade MeOH and MeCN were used for semipreparative isolation. LC−MS grade MeOH and MeCN were used for LC−MS analyses. Other chemicals used in the study were of analytical grade.

2.10. Culture of A549 cells and group design

A549 cells were purchased from Cell Resource Center of Peking Union Medical College, China. The cells were cultured in DMEM (Invitrogen, USA) supplemented with 10% fetal calf serum (Sijiqing, Hangzhou, China) and penicillin-streptomycin (Solarbio, Beijing, China) in a humidified atmosphere of 5% CO_2 at 37 °C. A549 cells were cultured as the control, sample, and reference groups. Compound **1** was added to the cells at different concentrations (10.85, 21.69, and 32.54 μmol/L), and adriamycin was added to the reference group (2.34 μmol/L, Sigma, USA) for 24 h. Cells were collected and used in various experiments after 24 h.

2.11. Detection of apoptosis by flow cytometry and ELISA

A549 cells were digested with 0.25% trypsin, washed twice with PBS at 4 °C, and resuspended in 0.5 mL of binding buffer. The cells were incubated with 10 μL of Annexin V/FITC (Solarbio, Beijing, China) at 4 °C in the dark for 60 min and with 5 μL of PI at 25 °C for 5 min. Fluorescence was analyzed using a FACS-Calibur flow cytometer (Becton-Dickinson, NJ, USA). Lysis and extraction of A549 cells were performed using RIPA lysis buffer (Solarbio, Beijing, China). Protein concentrations were assayed using a BCA protein kit (Pierce, USA). The levels of PI-3K and AKT were detected by ELISA kits (Huamei, Wuhan, China). All operations were performed according to the manufacturer's instructions for the kits. The absorbance of the samples was determined by a microplate reader (Molecular Devices, CA, USA).

2.12. Phylogenetic analysis

The internal transcribed spacer (ITS) sequences of fungal strains producing tyrosine-decahydrofluorene derivatives were aquired from the GenBank database and aligned using ClustalW software. A rooted neighbor-joining tree was generated using a Poisson model by MEGA 8.0 software with bootstrapping for 1000 replicates.

2.13. Statistical analysis

The data were analyzed using Adobe Illustrator CS6.0 and GraphPad Prism 8.0 software. The data are shown as the mean ± standard deviation. The experimental groups were compared by one-way ANOVA. P values < 0.05 was considered statistically significant.

3. Results and discussion

3.1. Identification and structural characterization of xenoacremones A−C (1−3)

Various fungal strains were screened for the production of tyrosine-decahydrofluorene derivatives under laboratory conditions. A novel fungal strain isolated from the Chinese mangrove (*Bruguiera gymnorrhiza*), *X. sinensis* ML-31, was identified as a candidate. This strain was cultured in rice medium for 7 days and then was extracted with EtOAc. LC−MS analysis of the crude extract revealed a predominant peak with $[M+H]^+$ ions at *m/z* 478.2563 with a deduced molecular formula of $C_{29}H_{36}NO_5$. The compound was identified as a new tyrosine-decahydrofluorene derivative named xenoacremone A (**1**) (Fig. 2). Comprehensive analysis of the 2D NMR sepctra confirmed the entire planar structure of **1**. The proton spin systems observed in the $^1H-^1H$ COSY spectra with cross-peaks from H-1 to H-15, and the HMBC correlations from H-7 to C-6, C-11, and C-13, and from H-14 to C-3, C-5, C-6, and C-15, were assigned to a decahydrofluorene moiety. Further HMBC correlations from H-1′ to C-3′, C-16, and C-18, from H-15 to C-17, together with from H-3′ to C-5′ and C-9′ completed the linkages of the phenyl, γ-lactam, and [6.5.6] tricarbocyclic moieties to form a 13-membered macrocyclic ether of **1**. The relative stereochemistry of **1** was elucidated based on the NOESY cross-peaks (Fig. 2B, Supporting Information Table S5, S24−S28). NMR and crystal X-ray diffraction analyses identified **3** as xenoacremone A (**1**) methyl ether, named xenoacremone C (**3**), which could have been formed spontaneously from **1** in methanol (Fig. 2A and B, Supporting Information Fig. S20 and Table S7). Compound **2** was determined to be $C_{29}H_{33}NO_5$ based on the HRESI-MS and NMR spectra as xenoacremone B containing a ketone group at C-16 and a ternary epoxide unit attached to the pyrrolidinone moiety (Fig. 2A, Supporting Information Figs. S29−S35 and Table S6). The NOESY cross-peaks of H-1'/H-3b' and H-9' indicated the same β-orientation of the hydrogens (Supporting Information Fig. S34).

3.2. Bioinformatics analysis and verification of gene cluster involved in biosynthesis of 1

The biosynthetic pathways of xenoacremone compounds identified in *X. sinensis* ML-31 were investigated by genome sequencing of the strain. The size of the genome was approximately 41.9 Mbp, and antiSMASH indicated the presence of 47 gene clusters for biosynthesis of secondary metabolites[28]. All clusters of *X. sinensis* ML-31 were tested to identify possible gene cluster related to biosynthesis of **1**. A hybrid PKS−NRPS cluster was identified as a top candidate gene cluster participating in the biosynthetic pathway of **1**. A seven-gene (*xenA-xenG*) 53.0 kbp locus within this cluster was identified as a top candidate for the putative biosynthetic gene cluster for xenoacremones (*xen*). Sequence analysis suggested that the genes encoded a hybrid PKS−NRPS (XenE), a hydrolase (XenA), a transcription factor (TF, XenB), an enoyl reductase (ER, XenG), and three hypothetical proteins (XenC, XenD, and XenF) with intriguing functions (Fig. 3A, Supporting Information Table S4). Further BLASTP analysis demonstrated that homologous *xen* gene clusters were conserved in various fungi, including *Phialocephala scopiformis*, *Colletotrichum salicis*, *Hyaloscypha bicolor*, *Thermothielavioides terrestris*, *Cordyceps javanica*, and *Penicillium oxalicum*. However, to the best of our knowledge, tyrosine-decahydrofluorene derivatives or their biosynthetic pathways were not reported in these strains.

The hybrid PKS−NRPS XenE is composed of partially reducing PKS domains (KS-AT-DH-cMT-KR-ACP) at the N-terminus and NRPS domains (C-A-T-R) at the C-terminus (Fig. 3A) and clearly differs from previously reported hybrid PKS−NRPS enzymes, whose structures contain a highly reducing PKS module[3,31]. To test the function of *xenE* in *X. sinensis* ML-31, the gene was substituted with a hygromycin B resistance expression cassette by using PEG-mediated protoplast transformation[32]. The mutants were verified by PCR and cultivated in rice media. Ultra-high performance liquid chromatography (UPLC) analysis of the crude extracts revealed complete disappearance of **1**−**3**, confirming the involvement of XenE in the biosynthesis of these compounds (Fig. 3B, ii). Previous studies have shown that most fungal hybrid PKS−NRPS enzymes, such as TenS[33,34] and EqxS[35], require a *trans*-acting ER for product release. Therefore, we subsequently deleted the putative ER-encoding gene *xenG* in *X. sinensis* ML-31, and this deletion resulted in disappearance of **1**−**3** (Fig. 3B, iii). This result suggested that the cooperation of the core enzyme XenE with the ER XenG is responsible for the formation of a key precursor of xenoacremones. However, the structure of this precursor could not be identified or deduced based on the deletion experiments. To determine the involvement of other genes of this cluster in the biosynthesis of **1**, we used a similar strategy to delete the *xenA*−*xenD* and *xenF* genes. The extracts from the deletion mutants were analyzed by UPLC (Fig. S2). The results revealed that **1** and **2** were absent in all Δ*xenB*−Δ*xenD* mutants and **1** and **2** were produced in the Δ*xenA* mutant. The production of another unknown compound **8** was enhanced, which was apparently linked to reduction in the levels of **1** (Fig. 3B, iv−viii). These results demonstrated that seven genes, *xenA*−*xenG*, are involved in the biosynthesis of **1**.

3.3. Compound 5 is the first key intermediate in the biosynthesis of 1

The genomic DNA sequence of *xenE* was introduced into *A. nidulans* LO8030 with or without *xenG* to generate the TZG10 and TZG9 mutants, respectively. There were no changes in the chemical profile of TZG9 compared with that of *A. nidulans* LO8030; however, two major peaks (**5** and **8**) and three minor peaks (**4**, **9**, and **10**) were detected in TZG10 (Fig. 3C, ii and iii). These results indicated that XenE and XenG are required for the

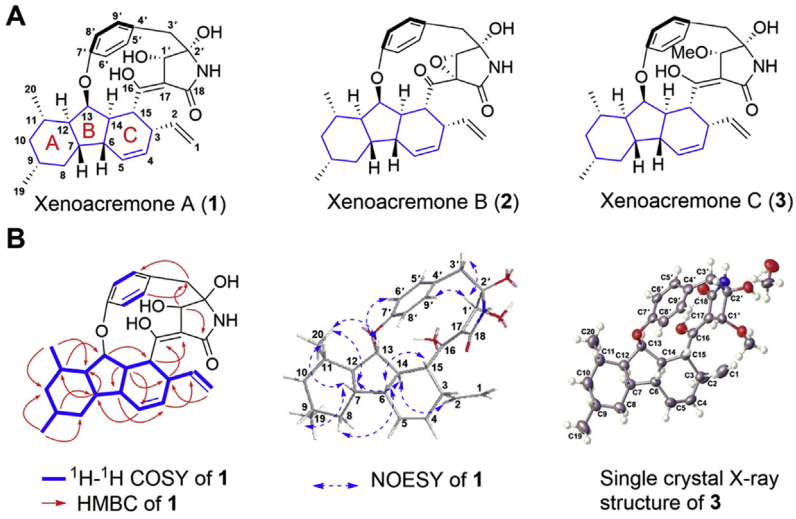

Figure 2 Structures and properties of xenoacremones A−C (**1**−**3**) isolated from *X. sinensis* ML-31. (A) Structures of xenoacremones A−C (**1**−**3**). (B) Elucidation of xenoacremones A and C (**1** and **3**).

formation of the core skeleton. Interestingly, deletion of the putative hydrolase xenA also resulted in the accumulation of **4**, **5**, and **8**−**10** and in a decrease in the amounts of **1** and another minor product, **11** (Fig. 3B, iv). Coexpression of *xenE* and *xenG* with *xenA* in *A. nidulans* LO8030 (TZG11) resulted in the accumulation of **5** and a decrease in the formation of **8** compared with those in TZG10 (Fig. 3C, iv). Scale-up fermentation of the Δ*xenA* mutant was used to prepare a crude EtOAc extract with a yield of 2.5 g. Isolation and structural elucidation proved that **8** ($[M+H]^+$ ion at *m/z* 466.2949) is a reduced tyrosine derivative containing a linear polyketide chain. Thus, we hypothesized that the alcohol group at C-2′ in **8** was formed by a reduction of the aldehyde group in **4** by a thioester reductase (R) domain, which catalyzed a strict two-electron reduction step to form an aldehyde group[36]. Nevertheless, **4** was unstable during the isolation procedure and might undergo a spontaneous reduction to alcohol **8**; alternatively, this reduction could have been catalyzed by an endogenous reductase outside of the *xen* cluster. These results demonstrated that the PKS module of XenE acted in combination with the *trans*-acting ER XenG to produce a double-methylated nonaketide attached to the T domain. In parallel, the A domain of the NRPS module activated L-tyrosine, which was then transferred to the T domain. The C domain subsequently linked this group to the polyketide chain, forming an enzyme-bound amide. Reductive release by the C-terminal R domain afforded the aldehyde derivative **4** (Fig. 4).

The results of LC−MS analysis revealed that **5**, **9**, and **10** are the isomers of a deduced molecule ($C_{29}H_{36}NO_3$ with $[M+H]^+$ ions at *m/z* 446.269 ± 0.005) and have different UV absorption characteristics. Comparison with the structures of **4** and **8** indicated that the structure of **5** included a pyrrolidone moiety, which was formed by intramolecular nucleophilic attack on the aldehyde group (Supporting Information Figs. S43−S49 and Table S8). The results of coexpression and structural analyses of TZG10 and TZG11 indicated spontaneous formation of **5** from **4**, and XenA hydrolase significantly accelerated this process. Incubation of **5** in acetonitrile resulted in the formation of compounds **9** and **10**, indicating that **5** is spontaneously converted during the extraction and isolation (Supporting Information Fig. S21). NMR analysis confirmed **9** and **10** as the decalin-containing products with different configurations (Supporting Information Figs. S70–S76 and S77–S83; Tables S12 and S13). We hypothesized that **9** and **10** were formed from **5** *via* spontaneous intramolecular Diels−Alder (IMDA) reactions. As mentioned above, the hybrid tyrosine-nonaketide intermediate acts as the key linear precursor to initiate multiple cyclization to afford GKK1032A$_2$, hirsutellone B, and pyrrocidine B[20,24,25]. Thus, we speculate that compound **5**, which contains a similar hybrid skeleton flanked with two methyl groups of *S*-adenosylmethionine added by the cMT domain, is an important precursor for subsequent cyclization.

3.4. *Compounds **6** and **7** are additional key intermediates in the biosynthesis of **1***

The *xenB*, *xenC*, *xenD*, and *xenF* genes were deleted in the ML-31 strain. The putative TF XenB was identified as a specific regulator that upregulated the expression of the *xen* genes because secondary metabolites completely abolished after *xenB* deletion (Fig. 3B, viii and Supporting Information Fig. S9). Individual deletions of *xenC*, *xenD*, or *xenF* resulted in abolishment of the end products **1** and **2** and accumulation of the putative biosynthetic precursor **5** and **5**-derived decalins (**9** and **10**) (Fig. 3B, v–vii and Supporting Information Figs. S10–S12). This result indicated that three enzymes (XenC, XenD, and XenF) are involved in the conversion of **5** to **2**. This process is significantly different from the one-step cyclization that produces full decahydrofluorene core and paracyclophane proposed in route iii (Fig. 1B). Moreover, detailed LC–MS analysis revealed that the major product **6** and the minor product **11** were detectable in the Δ*xenD* mutant (Fig. 3B, vi and Fig. S11). In addition to **6** and **11**, **7** was accumulated upon inactivation of *xenC* in *X. sinensis* ML-31. Appearance of these new accumulated peaks in *xenC* and *xenD* deletion mutants suggested that the compounds might be intermediates for the production of **2**. Subsequently, *xenEFG* and *xenAEFG* were coexpressed in *A. nidulans* (TZG12 and TZG13), respectively, to investigate the functions of these enzymes. The formation of **6** and **11** were detected in the two mutants, and was not detected in the *xenAEG* strain (TZG11) (Fig. 3C, iv–vi and Supporting Information Figs. S16 and S17). This finding indicated that XenF is involved in the formation of these intermediates.

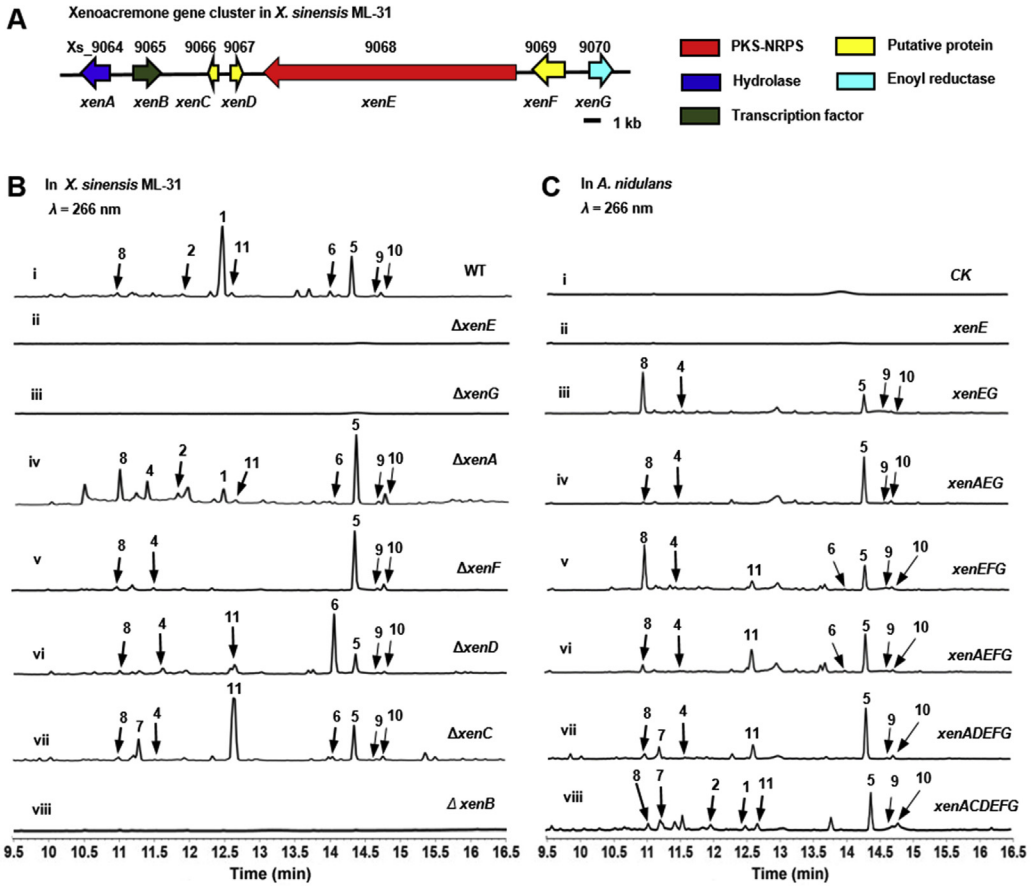

Figure 3 Identification of *xen* biosynthetic gene cluster and verification of the function of the *xenA*−*xenG* genes in *X. sinensis* ML-31. (A) Schematic representation of the xenoacremone cluster in *X. sinensis* ML-31. (B) The UPLC analysis of related compounds in *X. sinensis* ML-31 (wild type) and the mutant strains. Trace i, *X. sinensis* ML-31 (wild type strain producing) producing **1**−**2**, **5**−**6**, and **8**−**11**; trace ii, Δ*xenE*; trace iii, Δ*xenG*; trace iv, Δ*xenA* producing **1**−**2**, **4**−**6**, and **8**−**11**; trace v, Δ*xenF* producing **4**−**5** and **8**−**10**; trace vi, Δ*xenD* producing **4**−**6** and **8**−**11**; trace vii, Δ*xenC* producing **4**−**11;** trace viii, Δ*xenB*. (C) The UPLC analysis of related compounds in *A. nidulans* LO8030 mutant strains. Trace i, CK (*A. nidulans* LO8030); trace ii, *xenE*; trace iii, *xenEG* producing **4**−**5** and **8**−**10**; trace iv, *xenAEG* producing **4**−**5** and **8**−**10**; trace v, *xenEFG* producing **4**−**6** and **8**−**11**; trace vi, *xenAEFG* producing **4**−**6** and **8**−**11**; trace vii, *xenADEFG* producing **4**−**5** and **7**−**11**; trace viii, *xenACDEFG* producing **1**−**2**, **5**, and **7**−**11**. The peaks were detected by UV absorption at 266 nm.

Unlike TZG13, TZG19 harboring *xenADEFG* produced **7**, indicating that XenD catalyzed the formation of **7** (Fig. 3C, vii and Supporting Information Fig. S18). As expected, the end products **1** and **2** were detected in TZG20 harboring *xenACDEFG*, providing evidence for the involvement of XenC in end product formation (Fig. 3C, viii and Supporting Information Fig. S19).

Large-scale fermentation of the Δ*xenD* mutant in rice medium was performed to isolate compounds **6** and **11**. The results of NMR analysis revealed the formation of a new C−C bond between C-7 and C-12 of compound **6** to form a substituted hexane ring, which was not detected in **5** (Figs. S43–S49, and S50–S56, Supporting Information Tables S8 and S9). Surprisingly, the presence of a unique A-ring in **6** provided evidence for stepwise ring formation during biosynthesis of tricarbocyclic products. We speculated that XenF catalyzed [1,11]-sigmatropic rearrangement to accomplish the migration of σ-bond and subsequently install cyclohexane (Fig. 3C, v and vi and Fig. 4). This new enzyme was described to be involved in enhanced rearrangements during biosynthesis of secondary metabolites[32,37]. Compound **11** was identified as a pair of stereoisomers, **11a** and **11b** (Supporting Information Figs. S84−S90 and Tables S14 and S15). Structural elucidation suggested that **6** was converted to **11** by keto-enol tautomerization at C-16 and reduction of the C-1′−C-2′ double-bond (Fig. 4). However, the enzyme responsible for the reduction of **6** has not been identified. It cannot be excluded that this conversion occurred spontaneously or that the responsible gene may be located outside the *xen* cluster. The Δ*xenC* mutant was cultivated in rice medium, and the culture was extracted with EtOAc to afford a crude extract in a manner similar to that used for Δ*xenD*. LC−MS analysis revealed the presence of peak **7** with $[M+H]^+$ ions at *m/z* 478.2597. Comparison with **6** indicated that **7** possesses a ternary epoxide unit across C-1′ and C-17, a hydroxyl group at C-2′, and a ketone group at C-16 (Supporting Information Figs. S57−S62 and Table S10). This result indicated that XenD was responsible for hydroxylation and epoxidation of **6** to **7**, which was subsequently catalyzed by XenC. Structural comparison implied that the conversion of **7** to **2** required the installation of paracyclophane ether and subsequent IMDA reaction. Spontaneous IMDA reactions are involved in the biosynthesis of leporin, brevianamide A, and GB alkaloids[37−41]; thus, a spontaneous IMDA reaction may be able to afford rings B and C (Fig. 4). These findings suggested that XenC catalyzed the formation of

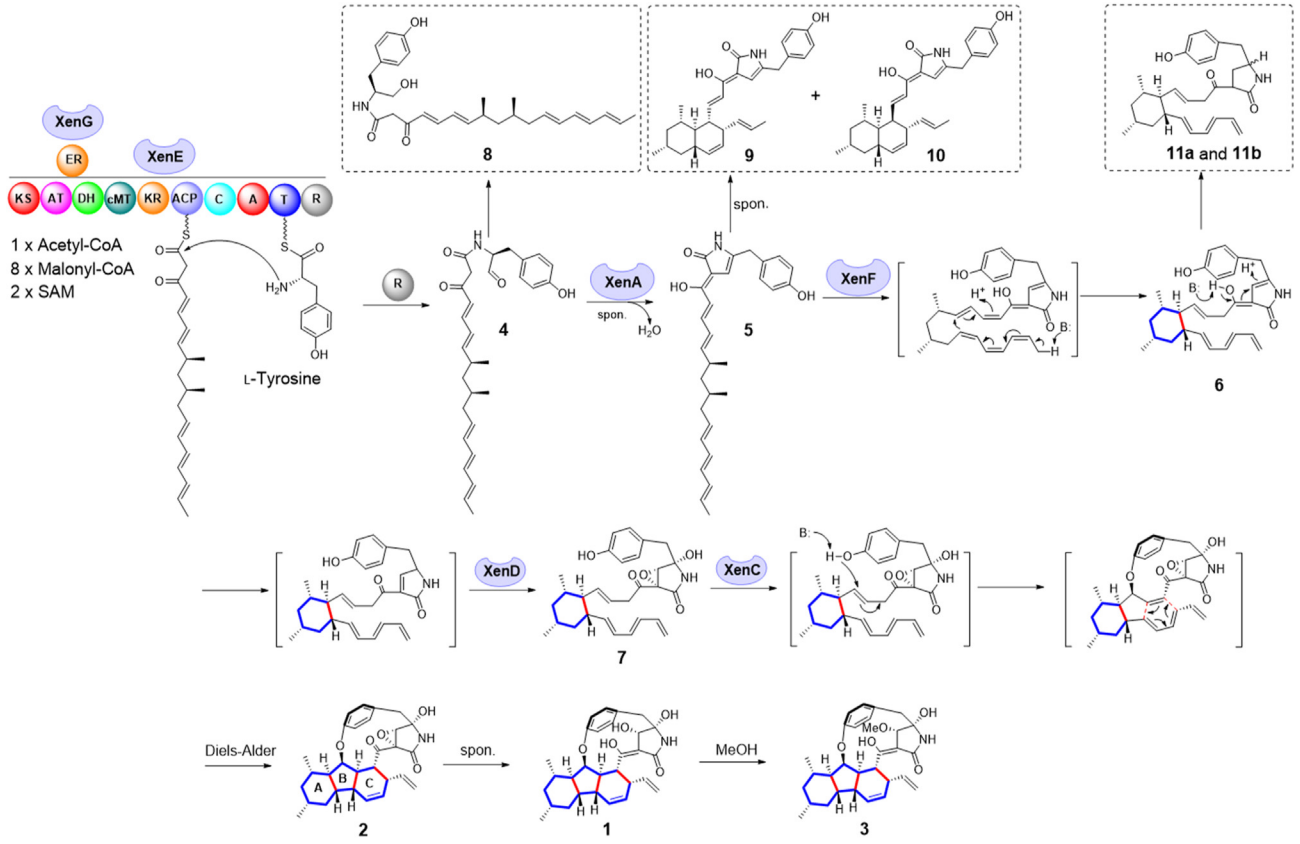

Figure 4 Proposed biosynthetic pathway of xenoacremones in *X. sinensis* ML-31.

paracyclophane ether to give the IMDA substrate. However, an intermediate paracyclophane derivative corresponding to a transition state was not detected due to instability.

3.5. *Bioactivity evaluation of* ***1***

The PI3K/AKT pathway is frequently altered in human cancer and involved in cell survival and anti-apoptotic signaling. Cell signaling regulated by PI3K/AKT is associated with cell proliferation, cell migration, and angiogenesis *via* induction of the NF-κB transcription factor. Treatment with xenoacremone A (**1**) (10.85, 21.69, and 32.54 μmol/L) increased the percentage of apoptotic cells to 30.68 ± 8.70%, 51.74 ± 7.95%, and 74.98 ± 10.44%, respectively. The results of ELISA revealed that the expression levels of PI3K and AKT were decreased in a dose-dependent manner compared with those in the control group. Flow cytometry results indicated that the apoptotic rate in control group was 5.32 ± 0.77% (Fig. 5A−H). The data of the present study indicated that compound **1** accelerated apoptosis of A549 lung cancer cells *via* the PI3K/AKT signaling pathway. These results demonstrated that the inhibitory activity of **1** toward the PI3K/AKT signaling pathway and the ability of **1** to induce apoptosis of A549 lung cancer cells.

4. Conclusions

In conclusion, we isolated three novel tyrosine-decahydrofluorene derivatives, xenoacremones A−C (**1**−**3**), from *X. sinensis* ML-31. Gene deletion in the native strain and heterologous expression led to identification of the corresponding biosynthetic gene cluster and elucidation of the biosynthetic pathway. Cooperation of the hybrid PKS−NRPS XenE and the *trans*-acting ER XenG is responsible for the formation of the reduced tyrosine-nonaketide derivative **4**. XenA accelerates intramolecular nucleophilic attack to give the pyrrolidone derivative **5**. Subsequently, three enzymes, XenF, XenD, and XenC, coordinately participate in the conversion of **5** to **2**. Surprisingly, XenF catalyzes sigmatropic rearrangement to form an A-ring, which leads to the unusual intermediate **6** with a hexane ring, which is required for the formation of the tricarbocyclic product. To the best of our knowledge, the formation of intermediate **6** with a hexane ring *via* cyclic enzymatic sigmatropic rearrangement is described for the first time in the biosynthesis of tyrosine-decahydrofluorene derivatives. Epoxidation of **6** to **7** catalyzed by XenD and the formation of the paracyclophane ether catalyzed by XenC initiate a spontaneous IMDA reaction to yield **2**. Spontaneous hydration of **2** leads to the formation of **1**, which undergoes subsequent methylation to afford **3** in methanol (Fig. 4). Our results identified three novel enzymes involved in several processes associated with the multiring formation of tyrosine-decahydrofluorene derivatives: installation of the A-ring, formation of the paracyclophane ether, and final fusion of rings B and C. The findings of the present study provide preliminary information on the biosynthesis mechanisms of tyrosine-decahydrofluorene derivatives and expand our knowledge of the biosynthesis of the [6.5.6] tricarbocyclic system to provide new insight into enzyme-mediated cascade cyclization in nature.

Acknowledgments

We thank Dr. Yanan Wang for all NMR data collection. We thank Drs. Zhengren Xu (Peking University) and Huomiao Ran for their

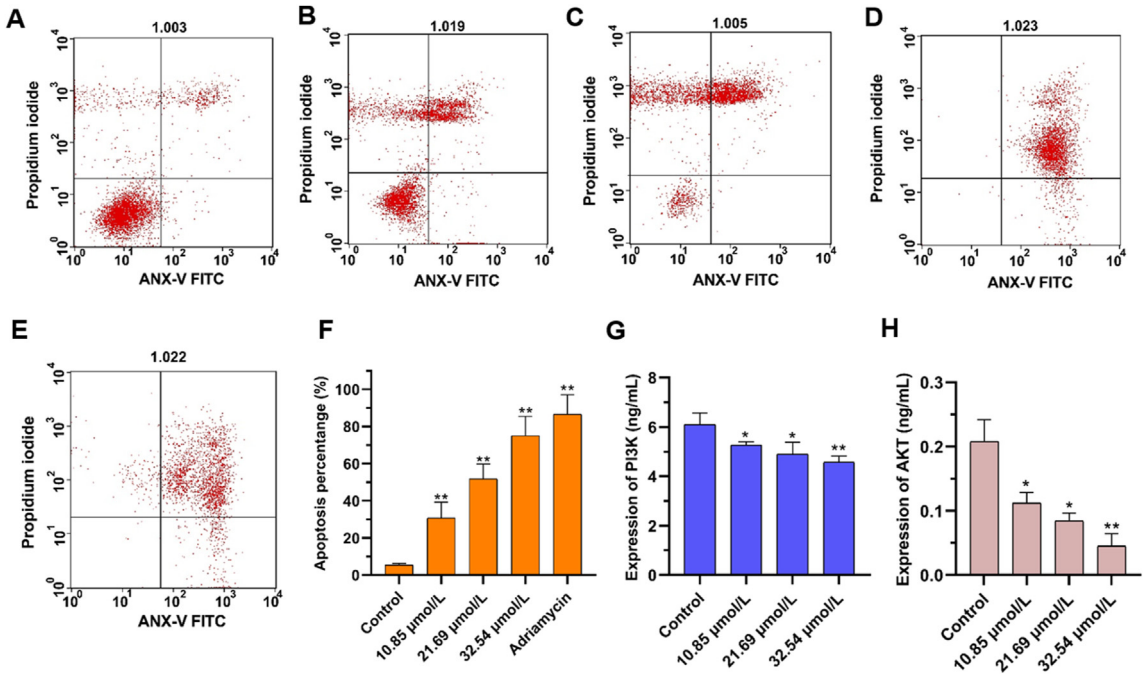

Figure 5 The apoptosis rate of A549 cells was detected by Annexin V/FITC staining and flow cytometry. (A) Control. (B) Compound **1** at 10.85 μmol/L. (C) Compound **1** at 21. 69 μmol/L. (D) Compound **1** at 32.54 μmol/L. (E) Adriamycin at 2.34 μmol/L. (F) The percentages of apoptosis induced by **1** and adriamycin are shown in the columns. (G) PI3K expressions in A549 cells measured by ELISA. (H) AKT expressions in A549 cells measured by ELISA. Data are presented as mean ± standard deviation, $n=3$ in each group. *$P < 0.05$ and ***$P < 0.01$ compared with the control group.

helpful discussions. This work was supported in part by National Key Research and Development Program of China (2020YFA0907800 and 2018YFC1706104), National Natural Science Foundation of China (31861133004 and 81502968), the Deutsche Forschungsgemeinschaft (DFG, German Research Foundation Li844/11-1, Germany) as well as Key Research Program of Frontier Sciences, CAS (ZDBS-LY-SM016, China).

Author contributions

Yi Sun, Shilin Chen and Wenbing Yin developed the hypothesis and designed the study. Zhiguo Liu and Peng Zhang constructed the plasmids. Zhiguo Liu and Wei Li constructed the mutant strains in the study. Zhiguo Liu and Yi Sun performed the compound isolation and characterization. Fangbo Zhang and Caixia Wang determinates the bioactivity. Zhiguo Liu, Jie Fan, Shuming Li and Wenbing Yin performed the biosynthetic pathway. Wenbing Yin, Wei Li, Zhiguo Liu, Yi Sun and Jie Fan performed the manuscript. All of the authors analyzed and discussed the results.

Conflicts of interest

The authors have no conflicts of interest to declare.

Appendix A. Supporting information

Supporting information to this article can be found online at https://doi.org/10.1016/j.apsb.2021.03.034.

References

1. Fisch KM. Biosynthesis of natural products by microbial iterative hybrid PKS−NRPS. *RSC Adv* 2013;**3**:18228−47.
2. Becker J, Liermann JC, Opatz T, Anke H, Thines E. GKK1032A$_2$, a secondary metabolite from *Penicillium* sp IBWF-029-96, inhibits conidial germination in the rice blast fungus *Magnaporthe oryzae*. *J Antibiot* 2012;**65**:99−102.
3. Isaka M, Rugseree N, Maithip P, Kongsaeree P, Prabpai S, Thebtaranonth Y. Hirsutellones A−E, antimycobacterial alkaloids from the insect pathogenic fungus *Hirsutella nivea* BCC 2594. *Tetrahedron* 2005;**61**:5577−83.
4. He HY, Yang HY, Bigelis R, Solum EH, Greenstein M, Carter GT. Pyrrocidines A and B, new antibiotics produced by a filamentous fungus. *Tetrahedron Lett* 2002;**43**:1633−6.
5. Hsiao SH, Wicklow D, Haschek W. Cytotoxicity of pyrrocidines in HepG2 hepatocytes and PK15 renal cells. *Toxicol Pathol* 2008;**36**:161−5.
6. Shiono Y, Kosukegawa A, Koseki T, Murayama T, Kwon E, et al. A dimeric pyrrocidine from *Neonectria ramulariae* is an inhibitor of prolyl oligopeptidase. *Phytochem Lett* 2012;**5**:91−5.
7. Shiono Y, Furukawa M, Koseki T, Kwon E, Kurniawan AH, Sato S, et al. A pyrrocidine derivative produced by fungus *Neonectria ramulariae* In-2 isolated from a Beetle *Holotrichia picea*. *Phytochem Lett* 2018;**26**:120−4.
8. Wicklow DT, Poling SM, Summerbell RC. Occurrence of pyrrocidine and dihydroresorcylide production among *Acremonium zeae* populations from maize grown in different regions. *Can J Plant Pathol* 2008;**30**:425−33.
9. Madla S, Isaka M, Wongsa P. Modification of culture conditions for production of the anti-tubercular hirsutellones by the insect pathogenic fungus *Hirsutella nivea* BCC 2594. *Lett Appl Microbiol* 2008;**47**:74−8.

10. Isaka M. Novel bioactive compounds from insect pathogenic fungi. *J Syn Org Chem Japan* 2007;**65**:700−8.
11. Song T, Chen M, Ge ZW, Chai W, Li XC, Zhang Z, et al. Bioactive penicipyrrodiether a, an adduct of GKK1032 analogue and phenol a derivative, from a marine-sourced fungus *Penicillium* sp. ZZ380. *J Org Chem* 2018;**83**:13395−401.
12. Qi X, Li X, Zhao J, He N, Li Y, Zhang T, et al. GKK1032C, a new alkaloid compound from the endophytic fungus *Penicillium* sp. CPCC 400817 with activity against methicillin-resistant S. aureus. *J Antibiot* 2019;**72**:237−40.
13. Asano M, Inoue M, Watanabe K, Abe H, Katoh T. Synthetic studies toward GKK1032s, novel antibiotic antitumor agents: enantioselective synthesis of the fully elaborated tricyclic core *via* an intramolecular Diels−Alder cycloaddition. *J Org Chem* 2006;**71**:6942−51.
14. Tilley SD, Reber KP, Sorensen EJ. A rapid, asymmetric synthesis of the decahydrofluorene core of the hirsutellones. *Org Lett* 2009;**11**: 701−3.
15. Nicolaou KC, Sarlah D, Wu TR, Zhan W. Total synthesis of hirsutellone B. *Angew Chem Int Ed* 2009;**48**:6870−4.
16. Huang M, Song L, Liu B. Construction of the cyclophane core of the hirsutellones *via* a RCM strategy. *Org Lett* 2010;**12**:2504−7.
17. Uchiro H, Kato R, Arai Y, Hasegawa M, Kobayakawa Y. Total synthesis of hirsutellone B *via* Ullmann-type direct 13-membered macrocyclization. *Org Lett* 2011;**13**:6268−71.
18. Nicolaou KC, Sun YP, Sarlah D, Zhan W, Wu TR. Bioinspired synthesis of hirsutellones A, B, and C. *Org Lett* 2011;**13**:5708−10.
19. Tanaka R, Ohishi K, Takanashi N, Nagano T, Suizu H, Suzuki T, et al. Synthetic study of pyrrocidines: first entry to the decahydrofluorene core of pyrrocidines. *Org Lett* 2012;**14**:4886−9.
20. Oikawa H. Biosynthesis of structurally unique fungal metabolite GKK1032A_2: indication of novel carbocyclic formation mechanism in polyketide biosynthesis. *J Org Chem* 2003;**68**:3552−7.
21. Ear A, Amand S, Blanchard F, Blond A, Dubost L, Buisson D, et al. Direct biosynthetic cyclization of a distorted paracyclophane highlighted by double isotopic labelling of L-tyrosine. *Org Biomol Chem* 2015;**13**:3662−6.
22. Walsh CT, O'Brien RV, Khosla C. Nonproteinogenic amino acid building blocks for nonribosomal peptide and hybrid polyketide scaffolds. *Angew Chem Int Ed* 2013;**52**:7098−124.
23. Miyanaga A, Kudo F, Eguchi T. Protein−protein interactions in polyketide synthase−nonribosomal peptide synthetase hybrid assembly lines. *Nat Prod Rep* 2018;**35**:1185−209.
24. Tang MC, Zou Y, Watanabe K, Walsh CT, Tang Y. Oxidative cyclization in natural product biosynthesis. *Chem Rev* 2017;**117**:5226−333.
25. Li XW, Ear A, Nay B. Hirsutellones and beyond: figuring out the biological and synthetic logics toward chemical complexity in fungal PKS−NRPS compounds. *Nat Prod Rep* 2013;**30**:765−82.
26. Li W, Fan A, Wang L, Zhang P, Liu Z, An Z, Yin WB. Asperphenamate biosynthesis reveals a novel two-module NRPS system to synthesize amino acid esters in fungi. *Chem Sci* 2018;**9**:2589−94.
27. Tang MC, Lin HC, Li D, Zou Y, Li J, Xu W, et al. Discovery of unclustered fungal indole diterpene biosynthetic pathways through combinatorial pathway reassembly in engineered yeast. *J Am Chem Soc* 2015;**137**:13724−7.
28. Blin K, Wolf T, Chevrette MG, Lu X, Schwalen CJ, Kautsar SA, et al. AntiSMASH 4.0-improvements in chemistry prediction and gene cluster boundary identification. *Nucleic Acids Res* 2017;**45**:W36−41.
29. Yin WB, Chooi YH, Smith AR, Cacho RA, Hu Y, White TC, et al. Discovery of cryptic polyketide metabolites from dermatophytes using heterologous expression in *Aspergillus nidulans*. *ACS Synth Bio* 2013; **2**:629−34.
30. Chiang YM, Ahuja M, Oakley CE, Entwistle R, Asokan A, Zutz C, et al. Development of genetic dereplication strains in *Aspergillus nidulans* results in the discovery of aspercryptin. *Angew Chem Int Ed* 2016;**55**:1662−5.
31. Boettger D, Hertweck C. Molecular diversity sculpted by fungal PKS−NRPS hybrids. *Chembiochem* 2013;**14**:28−42.
32. Prier CK, Hyster TK, Farwell CC, Huang A, Arnold FH. Asymmetric enzymatic synthesis of allylic amines: a sigmatropic rearrangement strategy. *Angew Chem Int Ed* 2016;**55**:4711−5.
33. Halo LM, Marshall JW, Yakasai AA, Song Z, Butts CP, Crump MP, et al. Authentic heterologous expression of the tenellin iterative polyketide synthase nonribosomal peptide synthetase requires coexpression with an enoyl reductase. *Chembiochem* 2008;**9**:585−94.
34. Eley KL, Halo LM, Song Z, Powles H, Cox RJ, Bailey AM, et al. Biosynthesis of the 2-pyridone tenellin in the insect pathogenic fungus *Beauveria bassiana*. *Chembiochem* 2007;**8**:289−97.
35. Sims JW, Fillmore JP, Warner DD, Schmidt EW. Equisetin biosynthesis in *Fusarium heterosporum*. *Chem Comm* 2005;**2**: 186−8.
36. Gahloth D, Dunstan MS, Quaglia D, Klumbys E, Lockhart-Cairns MP, Hill AM, et al. Structures of carboxylic acid reductase reveal domain dynamics underlying catalysis. *Nat Chem Biol* 2017; **13**:975−81.
37. Ohashi M, Liu F, Hai Y, Chen M, Tang MC, Yang Z, et al. SAM-dependent enzyme-catalysed pericyclic reactions in natural product biosynthesis. *Nature* 2017;**549**:502−6.
38. Evans DA, Adams DJ, Kwan EE. Progress toward the syntheses of (+)-GB 13, (+)-himgaline, and himandridine. new insights into intramolecular imine/enamine aldol cyclizations. *J Am Chem Soc* 2012;**134**:8162−70.
39. Yang B, Gao S. Recent advances in the application of Diels−Alder reactions involving *o*-quinodimethanes, aza-*o*-quinone methides and *o*-quinone methides in natural product total synthesis. *Chem Soc Rev* 2018;**47**:7926−53.
40. Ye Y, Du L, Zhang X, Newmister SA, McCauley M, Alegre-Requena JV, et al. Fungal-derived brevianamide assembly by a stereoselective semipinacolase. *Nat Catal* 2020;**3**:497−506.
41. Chen SL, Sun Y, Wan HH, Zhang H, Zhao QH. Highlights on the progress of traditional Chinese medicine and natural drugs during 2015−2020. *Acta Pharm Sin* 2020;**55**:2751−76.